

SCALE INVARIANT AVALANCHES: A CRITICAL CONFUSION

*Osvanny Ramos**

Laboratoire PMMH, ESPCI, CNRS UMR 7636,
10 rue Vauquelin, 75231 Paris Cedex 05, France.
Laboratoire PMCN, Université Lyon 1, CNRS UMR 5586,
43 Bld. du 11 novembre 1918, 69622 Villeurbanne, France

November 7, 2018

Abstract

The “Self-organized criticality” (SOC), introduced in 1987 by Bak, Tang and Wiesenfeld, was an attempt to explain the $1/f$ noise, but it rapidly evolved towards a more ambitious scope: explaining scale invariant avalanches. In two decades, phenomena as diverse as earthquakes, granular piles, snow avalanches, solar flares, superconducting vortices, sub-critical fracture, evolution, and even stock market crashes have been reported to evolve through scale invariant avalanches. The theory, based on the key axiom that a critical state is an attractor of the dynamics, presented an exponent close to -1 (in two dimensions) for the power-law distribution of avalanche sizes. However, the majority of real phenomena classified as SOC present smaller exponents, i.e., larger absolute values of negative exponents, a situation that has provoked a lot of confusion in the field of scale invariant avalanches. The main goal of this chapter is to shed light on this issue. The essential role of the exponent value of the power-law distribution of avalanche sizes is discussed. The exponent value controls the ratio of small and large events, the energy balance –required for stationary systems– and the critical properties of the dynamics. A condition of criticality is introduced. As the exponent value decreases, there is a decrease of the critical properties, and consequently the system becomes, in principle, predictable. Prediction of scale invariant avalanches in both experiments and simulations are presented. Other sources of confusion as the use of logarithmic scales, and the avalanche dynamics in well established critical systems, are also revised; as well as the influence of dissipation and disorder in the “self-organization” of scale invariant dynamics.

PACS 05.65.+b, 91.30.Ab, 45.70.-n, 45.70.Ht

*E-mail: osvanny.ramos@univ-lyon1.fr

Keywords: avalanches, scale invariance, Self-organized Criticality, avalanche prediction.

1. Introduction

“But he hasn’t got anything on,” a little child said.
Hans Christian Andersen in *The Emperor’s New Clothes*

Scale invariance pervades nature, both in space and time. In space, it is revealed through the ubiquity of fractal structures; and in time, with the presence of scale invariant avalanches. Avalanches can be seen as sudden liberations of energy which has been accumulated very slowly¹; and phenomena as diverse as earthquakes [1, 2, 3], granular piles [4, 5, 6, 7, 8, 9, 11, 11, 12], snow avalanches [13], solar flares [14], superconducting vortices [15, 16, 17, 18], sub-critical fracture [19], evolution [20], and even stock market crashes [21] have been reported to evolve through scale invariant avalanches. The signature of the scale invariance corresponds to a power-law in the distribution of avalanche sizes, however, the exponents of the power-laws present in general different values. In 1987, Per Bak and co-workers introduced the “Self-organized criticality” (SOC) as an explanation of scale invariance in nature [22]. The SOC proposes a mapping between scale invariant avalanches and critical phenomena, with the key axiom that the critical state is an attractor of the dynamics, provoking the self-organization of the system towards a critical state [23, 24].

However, the axiomatic manner in which the base of the theory was introduced, set SOC as a theory to be proved more than as a theory to develop. Many theoretical studies focused on mapping SOC into the formalism of critical points [25, 26, 27]; others, on developing models displaying SOC behavior [1, 15, 20], increasing the members of the SOC family. However, the number of experiments were rather small, and they focused mainly on validating the theory, where the main goal was to find power-law distributions of avalanches [4, 5, 6, 7]. The original work presented an exponent close to -1 (in two dimensions), while many of the experimental and numerical results displayed smaller values, i.e., larger absolute values of negative exponents. Regardless this difference, they were classified as SOC, having as a “heritage” all the critical properties of the original model, thus bringing a lot of confusion to the field of scale invariant avalanches. The main goal of this chapter is to shed light on this issue.

The essential role of the exponent of the power-law in the dynamics is the first subject of discussion. The exponent value controls the ratio of small and large events, the energy balance –required for stationary systems– and the critical properties of the dynamics. The causes and consequences of a logarithmic scale, which is a source of confusion affecting the distribution of earthquakes, are also discussed in this first part of the chapter. The second part corresponds to the analysis of avalanches in a well established critical system: the Ising model. In the third part, the study focuses on the critical properties of scale invariant avalanches, where a condition of criticality is introduced. In phenomena evolving through power-law distributed avalanches, a critical behavior leads to the unpredictability of the

¹A more general definition of avalanches is introduced in section 3.1.1..

dynamics [24]. However, as the exponent of the power-law decreases, there is a decrease of the critical properties, and consequently the system becomes, in principle, predictable. Prediction of scale invariant avalanches in both experiments and simulations are presented in the fourth part of the chapter. In the last part, the influence of dissipation and disorder in the “self-organization” of scale invariant dynamics is also discussed.

2. Classification of Scale Invariant Avalanches

2.1. Fractals and scale invariant avalanches: the role of the exponent value

The introduction of the fractal dimension by Benoît Mandelbrot in 1975 [28, 29] changed the way nature is perceived; and self-similar branched and rough structures became more intuitive and natural than the artificially smooth objects of traditional Euclidean geometry. The self-affine structure of a Romanesco broccoli (figure 1a) is an eloquent example of a natural fractal and if a tiny insect traverses the vegetable following a straight line, it will surprisingly find a very long route. The Koch curve [30] is a good representation of this path (figure 1b), and the distribution of sizes of its different self-similar parts, resulting from a triangular “bending” of the central part of every line, follows a power-law $P(s) \sim s^b$ with an exponent $b = -1.2619$ [29] (figure 1c). A similar analysis over a smooth path donates an exponent equal -1. The absolute value of the exponent characterizes the trajectory and provides its dimension, which is fractal in the case of the broccoli. This fractal dimension is the main concept of the theory introduced by Mandelbrot; and by using the approach of “filling the space”, it can be understood rather intuitively: a smooth line “fits” in one dimension, while the rougher the self-affine curve (the higher the fractal dimension), the closer it is to fill a two-dimensional space. For the same reason, self-affine surfaces, as the one of the broccoli, present fractal dimensions between 2 and 3.

Through the fractal dimension, the value of the exponent of the power-law plays an essential role in the structural scale invariance; however, in the case of scale invariant

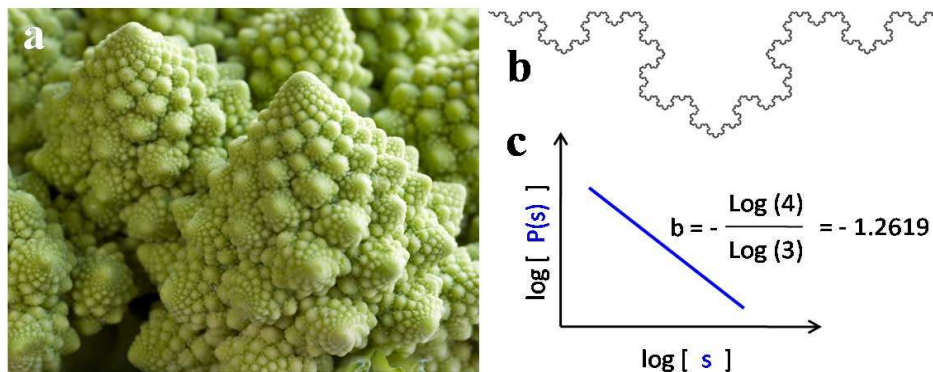


Figure 1. (a) Romanesco broccoli, an example of spatial scale invariance in nature (photo: O. Ramos). (b) The Koch curve as a representation of an intersection between a plane and the surface of the broccoli. (c) Scheme of the size distribution of the different parts in the structure of the Koch curve.

avalanches, the relevance of the exponent is much less understood. The earthquake dynamics is the phenomenon that normally comes to people's minds as the example of scale invariance in the temporal domain. Regardless the value of the exponent of the power-law distribution, the interpretation of scale invariance is limited to the absence of characteristic avalanches, and the existence of many small events and a few very large ones. Temporal relations between events are sometimes wrongly added to the interpretation, considering that there is no correlation between the different avalanches. The logarithmic scale in which the Gutenberg-Richter law was originally introduced [31] has also created confusion in the value of the exponent for the distribution of earthquakes, and consequently the implications of this value in the dynamics of scale invariant avalanches. Further down two examples with different exponents will clarify that, as in the case of fractal structures, the exponent of the power-law distribution *does* play a central role in the dynamics of scale invariant avalanches. However, first we will analyze how to classify scale invariant phenomena, where the historical use of a logarithmic scale has added some confusion to the interpretation of scale invariant avalanches.

2.2. The origin of logarithmic scales

All instruments operate with a finite characteristic resolution, which need to be consider seriously when analyzing data collected by the instrument. In a world permeated by scale invariance, how can one measure a variable presenting values over several orders of magnitude? The digital music, propelled by a technological revolution, has focused on increasing the resolution of the instruments [32]: 16 bits in a CD, 24 bits in a DVD, and up to 64 bits in internal processing. Being able to divide a signal into 32 bits ($4.294... \times 10^9$), or even into 64 bits ($1.844... \times 10^{19}$), is extraordinary; however, nature had to solve this problem with limited resolution², and therefore in an ingenious manner: by the application of scale transformations. Figure 2 illustrates several functions transforming a phenomenological scale of 10^9 levels of resolution into an instrumental scale of 8 bits of resolution (256 levels).

The function $y = x$ saturates the instrumental scale in less than three decades; while the function $y = cx$, although it covers the whole range of the phenomena, can not differentiate between values smaller than 10^6 . In order to find the best function let us introduce a generic transformation function $R(x)$ and its inverse $F(y)$. $R(x)$ gives the change in resolution due to the transformation and $F(y)$ provides the absolute error E_{abs} and relative error E_{rel} of the measurement:

$$E_{abs} \equiv dF(y)/dy, \quad E_{rel} \equiv E_{abs}/F(y). \quad (1)$$

Two cases are analyzed: (i) a power-law transformation and (ii) a logarithmic transformation:

$$(i) \quad R(x) = ax^b \quad (2)$$

$$F(y) = (y/a)^{1/b}, \quad E_{abs} = (1/b)(1/a)^{1/b} y^{(1/b)-1}, \quad E_{rel} = (1/b) y^{-1} \quad (3)$$

$$(ii) \quad R(x) = a \ln(bx) \quad (4)$$

²The human eye cannot distinguish between 256 grey levels [33].

$$F(y) = (1/b) \exp(y/a), \quad E_{abs} = (1/ab) \exp(y/a), \quad E_{rel} = 1/a \quad (5)$$

In the case of the power-law transformation, the absolute error depends on the value of the exponent. For $b = 1$ (linear case) E_{abs} is constant, for $b > 1$ it decreases with the measured value, thus the larger the value the more accurate the measurement. For $b < 1$, the absolute error increases with the measured value. If a phenomenon occurs over several orders of magnitude, only the case $b < 1$ can fulfil an instrumental scale with limited resolution. In the three cases the relative error decreases with the measured value. As a consequence, in the situation of a fractal structure as the one presented in figure 1; the larger the measured field, the larger the number of sublevels resolved by the measurement. Following this reasoning, if a digital camera is used as the instrument of measurement, as the camera moves apart in order to capture a larger structure, the number of pixels of the camera have to increase, a situation that is normal and common when one uses a tape measure: in order to measure a larger structure, the tape is enlarged and the number of units of measurement increase; thus the relative error decreases. This effect introduces a scale during the process of measurement, and allows knowing the size of the structure through the analysis of the relative error; thus, a power-law transformation “breaks” the scale invariance. However, the logarithmic transformation keeps constant the relative error. By using the same example, the resolution of the camera does not change when the camera moves apart, and there are no differences between two images taken at different scales. In this sense a logarithmic transformation respects the scale invariance, and this is the main reason for using this scale transformation in the classification of scale invariant phenomena.

Another reason is historical. In 1856 the English astronomer Norman R. Pogson proposed the current form of classification of the stars in different magnitudes in relation to the logarithm of their brightness [34]. He based the system on the work of Ptolemy [35], who probably based his work on the writings of the ancient Greek astronomer Hipparchus [36]. In 1860 the experimental psychologist Gustav T. Fechner proposed a logarithmic relation

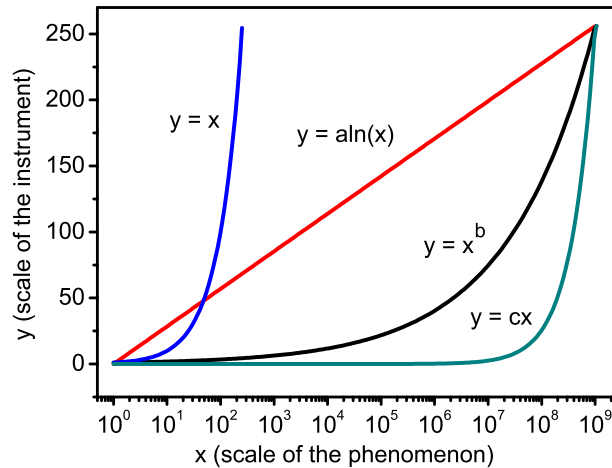


Figure 2. Different scale transformation from a phenomenon with 10^9 levels of resolution into an instrumental scale of 8 bits of resolution. $a = 256/\ln(10^9)$; $b = \ln(256)/\ln(10^9)$; $c = 256/10^9$.

between the intensity of the sensation and the stimulus that causes it [37]; so the thought logarithmic response of the human eye³ was responsible for the logarithmic nature of the stellar scale. In 1935 Charles F. Richter and Beno Gutenberg proposed a logarithmic scale to describe the earthquake's strength [39]. The name magnitude for this measurement came from Richter's childhood interest in Astronomy [40]; and the scale matches in some degree the earlier Mercalli intensity scale [41], which quantified the effects of an earthquake based on human perception.

2.3. Classifying scale invariant avalanches

Let us analyze now the two examples with different exponents. Two variables characterize the dynamics of power-law distributed avalanches: the value of the exponent of the power-law and the cut-off, which limits the maximum size of the events. In the following, the analysis will be simplified in considering a sharp cut-off at a value S_{max} .

$$P(s) = As^b \quad (6)$$

describes the pdf of the avalanches, where $1/A = \int_1^{S_{max}} s^b ds$ fulfils the condition of normalization $\int_1^{S_{max}} P(s) ds = 1$. Figure 3a shows the pdfs of two distributions of avalanche sizes with $S_{max} = 10^9$ and exponents $b = -1$ and $b = -2$. The distributions are represented in a log-log plot, and the avalanches are classified considering a logarithmic resolution: a "magnitude" m of the avalanches is defined as the logarithm of the avalanche size [$m = \log(s)$]; and the graph is divided into n equally spaced zones of m . For $n = 3$,

³More recent studies have proposed power-law relations between sensations and stimuli, experimentally proved in a rather narrow range of stimuli [38].

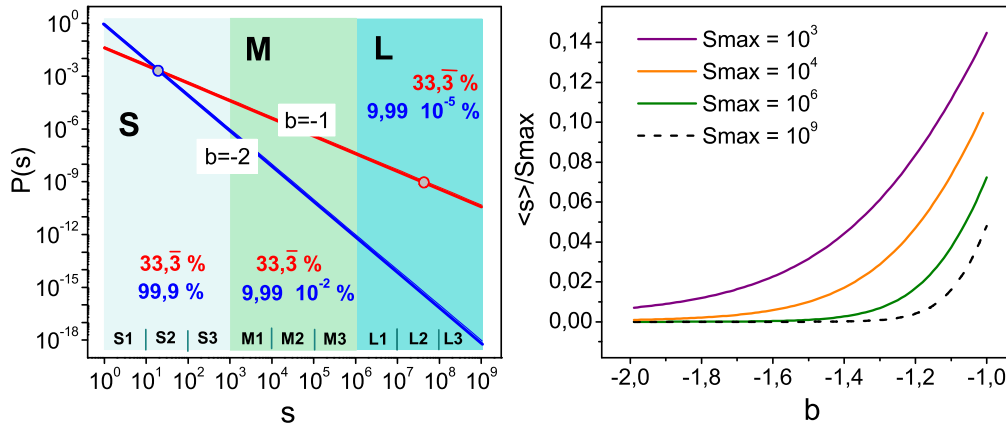


Figure 3. (a) Power-law distributions of avalanche sizes for two different exponent values: $b = -1$ and $b = -2$. The avalanches have been classified as small, medium and large following logarithmic bins. The percentage of each type of avalanche for the two different exponents is also displayed. A circle in each curve represents the mean value of the avalanche size $\langle s \rangle$. (b) Relation between the mean value of the avalanche size and the maximum avalanche size S_{max} as a function of b for different values of S_{max} .

avalanches smaller than $m = 3$ are considered small (S), those lying between $m = 3$ and $m = 6$ are medium (M), and those greater than $m = 6$ are large (L).

2.3.1. Integrated probability

The main confusion related to the logarithmic scale is a consequence of the fact that during the measurement, an integration has been already performed, which is well described through the integrated probability: $P_{Int}(s, k) = \int_s^{ks} A s^b ds$ calculates the probability of having an avalanche with size in the interval between s and ks . Due to the properties of the integral, the integrated probability is also a power-law with an exponent $b + 1$.

$$P_{Int}(s, k) = \frac{\ln(ks) - \ln(s)}{\ln(S_{max})} = \frac{\ln(k)}{\ln(S_{max})}, \quad b = -1 \quad (7)$$

$$P_{Int}(s, k) = \frac{(k^{b+1} - 1)s^{b+1}}{(S_{max}^{b+1} - 1)} \simeq (1 - k^{b+1})s^{b+1}, \quad -2 \leq b < -1 \quad (8)$$

The calculations performed with a value of $k = 10^3$ give the probabilities of the S, M and L avalanches shown in the graph of figure 3a. For $b = -1$ the integrated probability is constant and equal to $1/n$, so the three types of avalanches have the same probability equal to $1/3$. In the same manner, considering $k = 10$, the graph can be divided into decades: 9 zones equispaced in m that can be denominated as S1, S2, S3, M1, M2, M3, and L1, L2, L3 (shown in the graph), all of them with equal probability $1/9$. This situation, which evidently results from the logarithmic scale of measurement, is very far from the common interpretation of many small events and only a few very large ones; and in order to illustrate it more clearly, let us imagine the scenario of the distribution of earthquakes with an exponent equal to -1 : the consideration that one earthquake is happening every second gives in average one earthquake of magnitude between 2 and 3 (S3 in our scale) every 9^{th} second, but also a catastrophic quake of magnitude between 8 and 9 (L3 in our scale) every 9^{th} second. Fortunately, many real phenomena with catastrophic consequences have smaller exponents in their pdfs.

For $b = -2$, $P_{Int}(s, k) = (1 - k^{-1})/s$. Every decade the probability decreases by a factor 10. As a consequence, the probabilities of having a small avalanche is 0.999; 9.99×10^{-5} for a medium size avalanche; and only 9.99×10^{-7} for a large event (figure 3a). Again, if we imagine the scenario of the distribution of earthquakes with an exponent equal to -2 : the consideration that one earthquake is happening every second gives on average one minor earthquake of magnitude between 2 and 3 (S3 in our scale) every 111 seconds, one moderate of magnitude between 5 and 6 (M3 in our scale) every $1.1\bar{1} \times 10^5$ seconds (30,8 hours), and a catastrophic quake of magnitude between 8 and 9 (L3 in our scale) every $1.1\bar{1} \times 10^8$ seconds (3,5 years).

2.3.2. Mean value of avalanche size

Another relevant quantity signaling the key role of the exponent of the power-law, corresponds to the mean value of the size distribution of the avalanches $\langle s \rangle = \int_1^{S_{max}} sP(s)ds$.

$$\langle s \rangle = \frac{S_{max} - 1}{\ln(S_{max})}, \quad b = -1 \quad (9)$$

$$\langle s \rangle = \frac{(b+1) S_{max}^{(b+2)} - 1}{(b+2) S_{max}^{(b+1)} - 1}, \quad -2 < b < -1 \quad (10)$$

$$\langle s \rangle = \frac{\ln(S_{max})}{1 - S_{max}^{-1}}, \quad b = -2 \quad (11)$$

The mean value of the avalanche size is related to both the response of the system to a perturbation, and the energy balance in the dynamics. In the figure 3a, where $S_{max} = 10^9$, the values of $\langle s \rangle$ correspond to 4.8×10^7 and 20.7 for $b = -1$ and $b = -2$ respectively. These values are represented by a circle in each curve.

The value of $\langle s \rangle$ corresponds to the average response of the system to a perturbation, under the consideration that small perturbations can provoke the overcoming of local thresholds and thus the triggering of avalanches. In average, the system is delivering an avalanche of size $\langle s \rangle$; so in terms of avalanche production, this is equivalent to generate an avalanche of size $\langle s \rangle$ in every event of the dynamics. In the particular case of $\langle s \rangle$ proportional to the system size, the situation can be interpreted as critical: in average a perturbation provokes a response proportional to the system size. However, the fact that the dimension of the avalanche is smaller than the dimension of the system, adds some complexity to the analysis of the criticality through the avalanche size distribution, which will be discussed in section 4.1.1.

2.3.3. Energy balance in slowly driven systems

As mentioned in the introduction, avalanches are defined as sudden liberation of energy that has been accumulated very slowly. This indicates that the energy is injected in small portions, and that there is a separation between the drive of the system (slow) and the avalanche duration (rapid). At every single time interval, it is possible to define an injected energy, an avalanche of a particular size, and a dissipated energy. If the system is in a stationary state, the average energy injected to the system in every time interval has to be equal to the average dissipated energy. Consequently, the average dissipated energy has to be small,

$$\langle E_{injected} \rangle = \langle E_{dissip} \rangle. \quad (12)$$

Many of the models dealing with scale invariant avalanches are non-dissipative in the bulk, and the energy is liberated through the boundaries of the system [22]. However, they still refer as avalanches the local processes related to rearrangements in the bulk of the system, with no energy cost. As the avalanche production is not directly related to the dissipation of energy, these systems can have a large value of $\langle s \rangle$ and still present a small average value of the dissipated energy $\langle E_{dissip} \rangle$.

However, the vast majority of real phenomena are dissipative. Considering that

$$\langle E_{injected} \rangle \sim S_{min} \ll S_{max}, \quad \text{and} \quad \langle E_{dissip} \rangle = \alpha \langle s \rangle, \quad (13)$$

where α is a dissipation coefficient,

$$\alpha \langle s \rangle \ll S_{max}. \quad (14)$$

The larger the avalanche size, the larger the dissipation; and as a consequence, large values of $\langle s \rangle$ are forbidden for dissipative slowly driven system. Figure 3b shows the relation $\langle s \rangle / S_{max}$ for different b values, indicating that large values of b (close to -1) are forbidden for dissipative slowly driven system.

The previous analysis did not consider the existence of avalanches of size zero (let us call them *zero* avalanches), where the addition of energy to the system provokes no response in terms of avalanches ($s < S_{min}$). In order to compensate the energy lost for an average *non-zero* avalanche $\langle s \rangle$, the system needs a number n_{S0} of *zero* avalanches proportional to $\alpha \langle s \rangle / S_{min}$. For small b values, and thus small $\alpha \langle s \rangle$, n_{S0} can be the consequence of a lack of resolution in the measurement.

2.3.4. The distribution of earthquakes

The Gutenberg-Richter law [31] is the best known example of scale invariant avalanches. However, many studies from the Statistical Physics point of view have not considered the fact that the original distribution was measured in a logarithmic scale, which provokes a change equal -1 in the measured exponent [2, 42]. Other reports attribute this change to a cumulative manner in the definition of the probability [43], which is mathematically correct, but it is not the right interpretation; and it brings confusion to the Geological community [44].

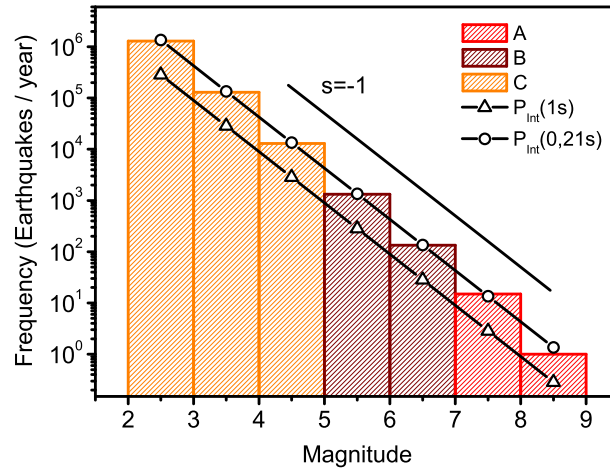


Figure 4. Frequency of earthquake occurrence worldwide. Data from the U.S. Geological Survey [45]: (A) Based on observations since 1900. (B) Based on observations since 1990. (C) Estimated. A solid line with slope $s = -1$ serves as a guide. The solutions of the Integrated probability for $b = -2$, considering that one earthquake occurs every second, and every 0.21 seconds, are also displayed.

Figure 4 displays the frequency of earthquake occurrence worldwide. The fact that the results are presented in intervals of magnitude indicates that the distribution corresponds to the integrated probability $P_{Int}(M_L)$, where M_L is the local magnitude. The graph shows that $\log[P_{int}(M_L)] \sim -M_L$. By substituting M_L into the definitions

$$M_L \equiv \log(A) + \text{const} \quad (15)$$

$$M_L \equiv 2/3 \log(E) + \text{const} \quad (16)$$

where A (wave amplitude) is the maximum excursion of the Wood-Anderson seismograph, according to the original work of Richter [39], and E the energy released by a quake, one gets $P_{Int}(A_L, 10) \sim A^{-1}$ and $P_{Int}(E_L, 10) \sim E^{-2/3}$. By adding -1 to the values of the exponents in the integrated probability, as discussed earlier (section 2.3.1.), it is possible to obtain the distributions of earthquakes in terms of A and E :

$$P(A) \sim A^{-2}, \quad P(E) \sim E^{-5/3} \quad (17)$$

In order to illustrate the integrated probability for the distributions of figure 3 (section 2.3.1.), the consideration of one earthquake happening every second was used. The results of this assumption for the case $b = -2$ are plotted in figure 4, and they are a little lower than the real values. However, the same analysis under the consideration of one earthquake occurring every 0.21 seconds fits quite well the real data (figure 4).

3. Avalanches in Critical Phenomena

The original motivation of this section was to study the properties of the scale invariant avalanches in well established critical systems, in order to compare them with the SOC avalanches. As discussed in the introduction, the SOC borrowed the concept of critical point of equilibrium phase transitions in order to describe their uncorrelated power-law distributed avalanches. The term *critical* in the avalanche context has been presented through the fact that at any moment a minor perturbation can trigger a response (avalanche) of any size and duration, a behavior that is linked to a divergence of the correlation length in the original numerical model of SOC: the BTW model [22]. Many dissipative phenomena involving avalanches distributed according to power-laws have been treated as critical systems [23, 24]; however, recent studies have shown different systems evolving through power-law distributed avalanches in a non-critical behavior [12, 46, 47], which has motivated the analysis of the avalanche dynamics in a well established critical scenario: a second order phase transition.

In Physics, the classical scenario of critical phenomena takes place during a second order phase transition [48]. The text-book example is the transition where a permanent magnet loses its magnetism: its magnetic properties cease when the temperature is increased above a certain critical temperature T_c . Below this temperature, a majority of spins point in the same direction, creating a magnetic field. Large fluctuations in spins do not occur at low temperatures, thus the system will remain unchanged. Above the critical temperature the spins' directions are random and change direction randomly, frequently and individually. The system is already disordered, therefore, no large-scale changes will happen; there is no overall magnetic field. However, at the critical temperature itself, large fluctuations occur and different snapshots of the system show different patterns - but all of the patterns will be statistically similar, in that clusters of aligned spins are surrounded by areas with spins oriented in the opposite direction. The clusters are of all sizes and their distribution follows

a power-law [49]. Four characteristic of this critical state will be used in our analysis along this chapter:

a) Divergence of the correlation length (ξ): The temporal average of the spatial auto-correlation function

$$\langle C_{As}(d, t) \rangle_t = \left\langle \frac{\sum f(x, y)f(x', y') - \langle f(x, y) \rangle^2}{\sum (f(x, y) - \langle f(x, y) \rangle)^2} \right\rangle_t \quad (18)$$

where $f(x, y)$ represents the structure of the system (in two dimensions) and d corresponds to the distance between (x, y) and (x', y') , can generally be fitted ($\forall T \neq T_c$) as an exponential decay in the form

$$\langle C_{As}(d, t) \rangle_t \sim \exp(-d/\xi). \quad (19)$$

At the critical point, the correlation length ξ is proportional to the linear size of the system L (diverging in an infinite system). The temporal average is necessary because the calculus is performed in a snapshot of the dynamics (a microstate), and any physical measure implies an average over many different microstates, which is equivalent to a temporal average if the system is ergodic [50].

b) Divergence of the correlation time (τ): The temporal autocorrelation function

$$C_{At}(t) = \frac{\sum f(t_i)f(t_i + t) - \langle f(t_i) \rangle^2}{\sum (f(t_i) - \langle f(t_i) \rangle)^2} \quad (20)$$

can be fitted as an exponential decay in the form

$$C_{At}(t) \sim \exp(-t/\tau). \quad (21)$$

Far from the critical point, the correlation time τ is small, so the system will quickly recover from a perturbation. At the critical point, τ diverges due to the fact that the system hesitates between the two states, and perturbations can move the system away from its equilibrium state during long periods of time. As a result, the dynamics turns slow, a phenomenon which is known as *critical slowing down* (CSD) [50].

c) Both ξ and τ present power-law dependencies with the reduced temperature $T_r = (T - T_c)/T_c$ in the way $\xi = |T_r|^{-\nu}$ and $\tau = |T_r|^{-z\nu}$; and thus they relate to each other through $\tau = \xi^z$. ν is called a *critical exponent* and is an attribute of the Ising model. Phenomena with the same critical exponents belong to the same universality class. The exponent z is often called the dynamic exponent. It gives a way to quantify the CSD and it depends on the algorithm, i.e., it depends on the type of dynamics [50].

d) As the size of the system increases, the transition between the two states becomes sharper, and it is infinitely sharp in an infinite system [50].

3.1. Avalanches \neq fluctuations

3.1.1. Simulation: the Ising model

In this subsection, the dynamics of avalanches is studied in a well established critical system: the Ising model, which is certainly the most thoroughly researched model in the whole

of statistical physics. It is a model of a magnet, and consists of a lattice where every site represents a spin of unit magnitude taking two values ± 1 as an indication of the only two possible directions to point: “up” or “down”. The spins interact with their nearest neighbors and the magnetization M is the sum over all the spins. For two or more dimensions the system shows a second order phase transition at a critical temperature T_c ($T_c = 2.269$ in two dimensions) from a ferromagnetic to a paramagnetic state when the temperature is increased, and in two dimensions the model is analytically solved [51]. The behavior of the average fluctuations of the magnetization is well known, and it defines the magnetic susceptibility, as well as its relation with the correlation function. The fluctuations of the magnetization ($M - \langle M \rangle$) have also been studied [52], and their pdf is reported to be universal [53]. It presents an exponential tail on one side, and a rapid falloff on the other side. However, in the scenario of SOC systems, instead of analyzing the fluctuations of the magnitudes, the standard is to define avalanches, corresponding to relative differences between consecutive states. Therefore, the definition of avalanches presented in the introduction, which is relative to slowly driven system, has been extended to *differences between equispaced values in the time series of the measured variable*. In the case of the Ising model, they corresponds to jumps in the magnetization between two consecutive microstates. Small simulations, both in size and in running time, will be sufficient to illustrate the dynamics of avalanches in this critical scenario.

The simulations take place in a 128×128 lattice with periodic boundary conditions, and compute 10^6 Monte Carlo steps (MCS) after 10^5 thermalization steps. Both Metropolis [55] and Wolff [56] algorithms are implemented considering no external magnetic field. Thus the energy of the system reads as $E = -J \sum_{\langle i, j \rangle} s_i s_j$ where $J = 1$ is a coupling constant and $\langle i, j \rangle$ indicates that the sum is over nearest neighbors only. In the Metropolis algorithm one MCS consists of $N = (128)^2$ events where one random spin is selected, and flipped ($s_i = -s_i$) if $\exp(-\Delta E/KT)$ is larger or equal to a random number between 0 and 1. ΔE is the change in energy due to the flip of the spin, and K is considered equal to 1, so the temperature T is presented as an adimensional magnitude. In the Wolff algorithm, one

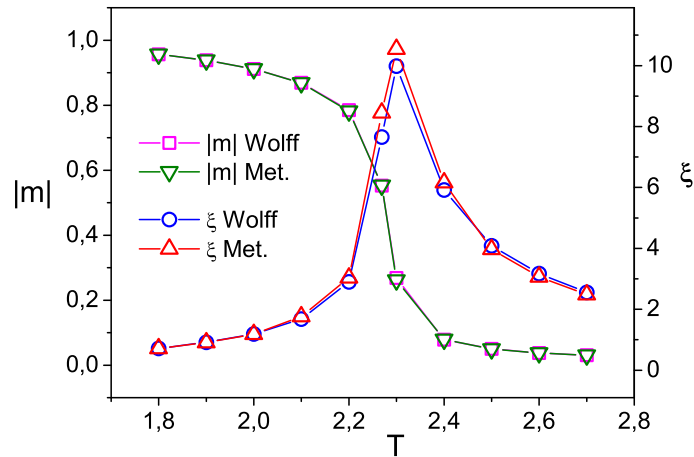


Figure 5. Average of the absolute value of the magnetization per spin and correlation length for both Metropolis and Wolff algorithms at different temperatures.

MCS consists of building up a cluster of flipped spins. Starting from flipping one spin at a random position, its neighbors will become part of the growing cluster if $\exp(-2J/KT)$ is smaller than a random number between 0 and 1.

The average of the absolute value of the magnetization per spin m , and the value of the correlation length ξ are shown in figure 5. The correlation length has been extracted following the eqs. 18 and 19:

$$\langle C(r) \rangle_t = \left\langle \frac{\sum_{d(i,j)=r}^N (s_i s_j) - m^2}{\sum_{d(i,j)=r}^N (s_i |s_j| - m)^2} \right\rangle_t \quad (22)$$

$$\langle C(r) \rangle_t \sim \exp(-r/\xi). \quad (23)$$

The correlation function has been calculated by using periodic boundary conditions, through an average of values taken every thousand MCS, and the sum is over those sites that are separated from each other by a distance equal to r . Both algorithms give very similar results on the averages of the physical magnitudes, with a peak in the correlation length coinciding with the phase transition.

The behavior of the fluctuations for the Wolff algorithm is presented in figure 6. For very low temperatures two symmetric Gaussian distributions (GDs) in the pdf of the magnetization indicate the two symmetric ordered states in the system (not shown in the graph).

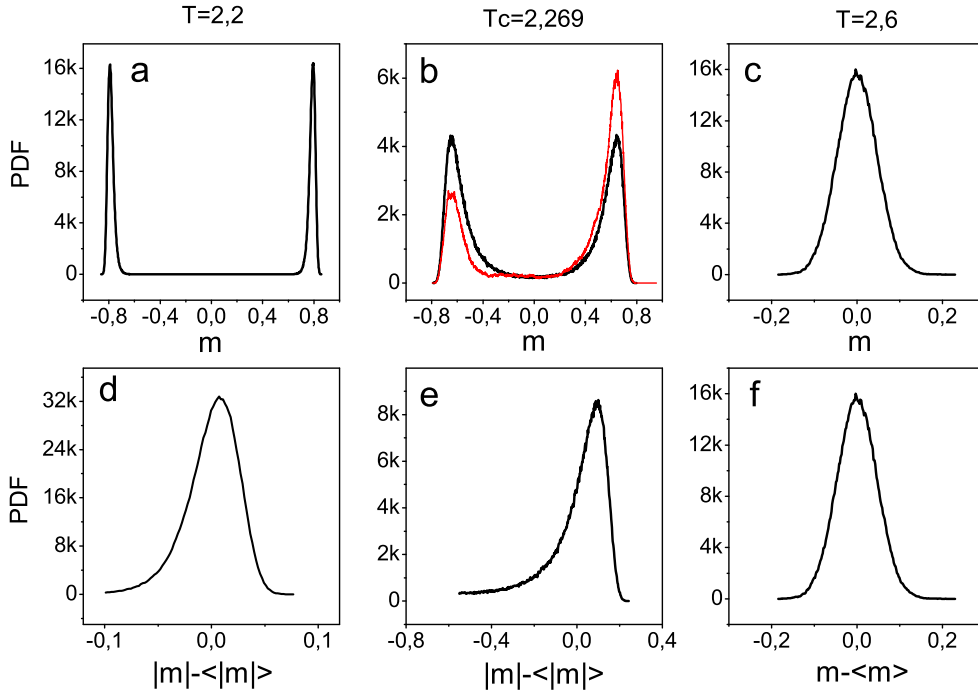


Figure 6. (a-c) Distribution of the magnetization for the Wolff algorithm at different temperatures. At the critical point, the distribution for the Metropolis algorithm is also displayed (b), presenting an asymmetric behavior. (d, e) Distribution of the fluctuations of the absolute value of the magnetization for the Wolff algorithm at different temperatures. (f) Distribution of the fluctuations of the magnetization for the Wolff algorithm at $T=2.6$.

As the temperature increases, the two GDs approach each other (figure 6a) and a small asymmetry starts to be noticed at the low frequencies in the pdf of the fluctuations of the absolute value of the magnetization (figure 6d). At the critical point, the two GDs start to merge forming the universal Gumbel distribution reporter by Bramwell *et. al.* in the pdf of the fluctuations of the absolute value of the magnetization [53, 54] (figure 6e). This Gumbel distribution of the fluctuations has been used by different experiments as an indication of the *criticality* of the system [57, 58]. For high temperatures we can consider that the two GDs have perfectly merged, and there is a Gaussian behavior of the fluctuation of the magnetization (figure 6f). In the case of the Metropolis algorithm only one side of the graph (a) will be explored by the system in a finite time (either positive or negative magnetization). The asymmetry displayed by the Metropolis algorithm in the graph (b) is a consequence of its slow dynamics, as it will be discussed further down. 10^6 MCS are not enough for the system to spend on average the same “time” in symmetrical areas of the phase space (with 10^7 MCS both algorithms have given the same result). The other graphs (c–f) are the same for both algorithms; consequently, they give the same results concerning the fluctuations of the absolute value of the magnetization.

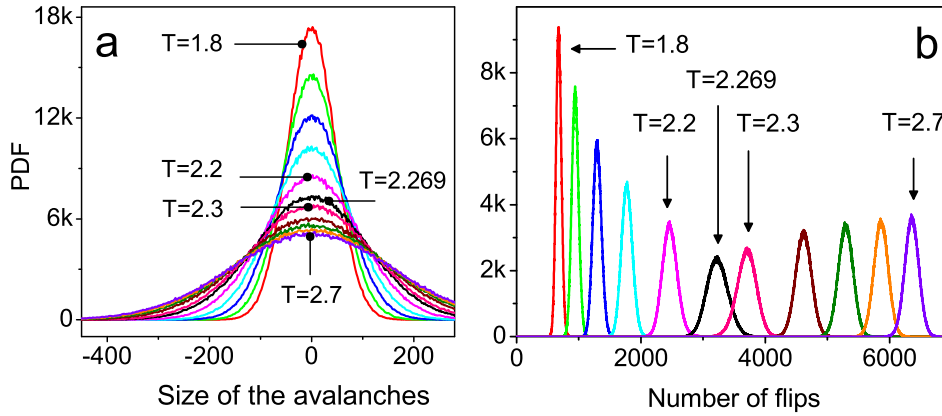


Figure 7. a) Distribution of the jumps in the magnetization (avalanches) for different temperatures (T) with the Metropolis algorithm. The curves correspond to T values between 1.8 and 2.7 with spacings of 0.1, and also the critical point: $T_c = 2.269$. b) Distributions of flips for different temperatures.

The distributions of the jumps of M (avalanches) and the distributions of flips for the Metropolis algorithm are displayed in figure 7. The avalanches follow a Gaussian for every measured T , and the distributions widen as T increases (figure 7a). The distributions of flips (figure 7b) also follow Gaussian distributions, with their mean values increasing with T and standard deviations having a maximum at the critical value $T_c = 2.269$.

The jumps of M in the Wolff algorithm (avalanches) are displayed in figure 8. The way that clusters build-up makes the absolute value of the jumps of M equal to the number of flipped spins, so only the distributions of avalanches are presented. As T decreases from the critical point the distributions display an increasing number of events that involve the whole system, which is an artefact. They have been removed from the graph and will not be taken into account in the analysis. At the critical temperature the avalanches follow a power-law

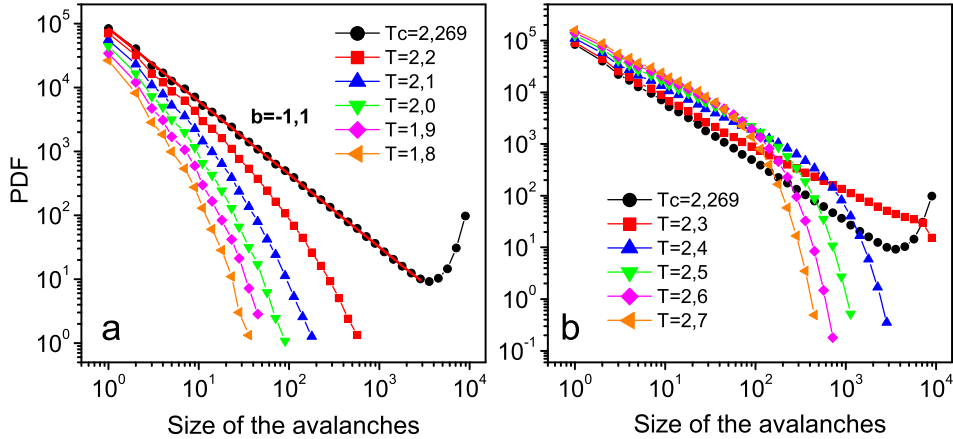


Figure 8. Distributions of the jumps of the magnetization (avalanches) for the Wolff algorithm at different temperatures.

distribution with an exponent $b = -1.1$. The distributions deviate from power-laws as the temperature moves away from T_c .

The analysis of the simulations has demonstrated that power-law distributed avalanches are not a necessary condition in order to classify a system as *critical*, but different kinds of distributions can rule the avalanche behavior of an equilibrium system at the critical point. The Metropolis dynamics at T_c is ruled by avalanches whose sizes are distributed following a Gaussian with standard deviation much smaller than the system size. It is a local dynamics happening on (and slowly re-shaping) a globally correlated landscape. Small jumps will move the system slowly around the phase space, so in a real situation a fast enough measurement can get the system “trapped” on a fluctuation, even far from the equilibrium value (calculated after a long enough averaging). This slow dynamics is directly linked to the CSD, situation which has been artificially eliminated in the Wolff algorithm. The Wolff dynamics at T_c is the one that people working with SOC models are accustomed to: avalanches that follow the landscape in an “invasion” mode, cascading through the system and resembling the properties of the globally correlated landscape. This direct relation between structure and avalanches is the key that allows analyzing the critical properties of a system from the characteristics of its scale invariant distribution of avalanches.

Two questions emanate from this analysis. The first: Is there an “algorithm” (a dynamics) chosen by nature? And the second: Is there CSD in real critical systems evolving through scale invariant avalanches? Let us discuss some experimental results.

3.1.2. Experiments: from the micro to the macro-world

The Wolff algorithm is much faster than the Metropolis one around T_c . This was a big achievement in 1989, where the computing capabilities were rather limited. However, it is well known that Metropolis represents better the dynamics of the second order phase transition around the Curie temperature [59]. The reason for that is the fact that many other less stronger interactions have not been considered in the analysis. They are included

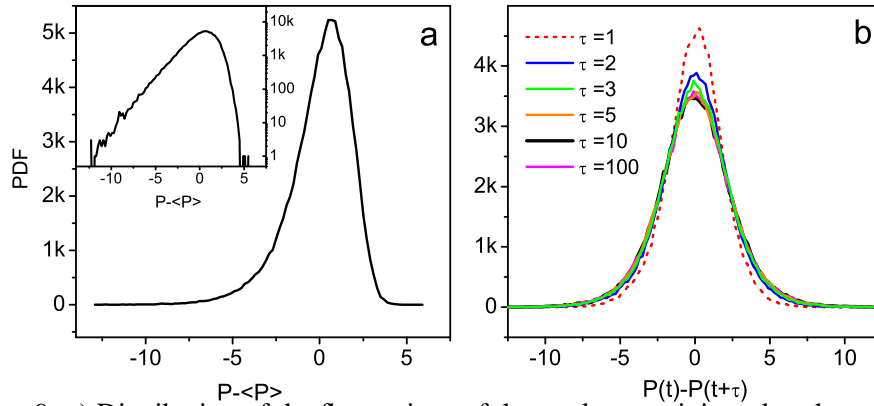


Figure 9. a) Distribution of the fluctuations of the total power injected to the motors of the rotatory disks in a turbulent flow experiment. Inset: The same function in log-lin axes, in order to enhance the asymmetry of the Gumbel. b) Distributions of avalanches for different τ values.

in something denominated *thermal bath* which tries to equilibrate the dynamics. Recent experiments have focused on the non-gaussian (Gumbel) distribution of fluctuations close to the Fréedericksz transition, a second order phase transition in a liquid crystal [57], and they have also confirmed the Gaussian character of the avalanche distributions close to the critical point [60]. However, if the system is kept at a low temperature (below T_c) and an external magnetic field is applied, the spins try to align themselves with the external field, and a reorganization of the magnetics domains takes place. This reorganization is not a smooth process, but is composed of small bursts or avalanches distributed following a power-law; a phenomenon which has been widely studied from the avalanche context [61, 62, 63] and is known as the Barkhausen effect [64].

Moving towards the macro-world, a turbulent flow is another phenomenon where non-gaussian fluctuations have been reported [54, 65]: two coaxial disks counter-rotate at a fixed velocity generating a swirling flow in the gap between them. The power required to keep a constant velocity of the disks (through a feedback loop) is measured and the fluctuations of the power correspond to the variable of analysis. If the experiment is performed inside a cylinder coaxial with the disks but with a diameter much larger than the disks' diameter, the fluctuations of the total power follow a Gaussian distribution. However, if the diameter of the cylinder is only slightly larger than the disks' diameter, the fluctuations of the total power follow a Gumbel distribution. The data presented in [54] have been reanalyzed for this chapter (courtesy of J.-F. Pinton): avalanches have been defined as relative differences between two points separated a time interval τ in the time series of total power. While the fluctuations of the total power display a Gumbel distribution (figure 9a), interpreted as a signature of a critical scenario; the avalanches follow a Gaussian distribution for all the different τ values (figure 9b). A remarkable difference in relation to the Ising model is the fact that the standard deviations of the Gaussian distributions are comparable to the width of the Gumbel. By following the same reasoning used in the Ising model, the Gumbel can be explained as the merging of the two Gaussian distributions of the fluctuations of the individual disks due to the confinement, which reduces the number of degrees of freedom

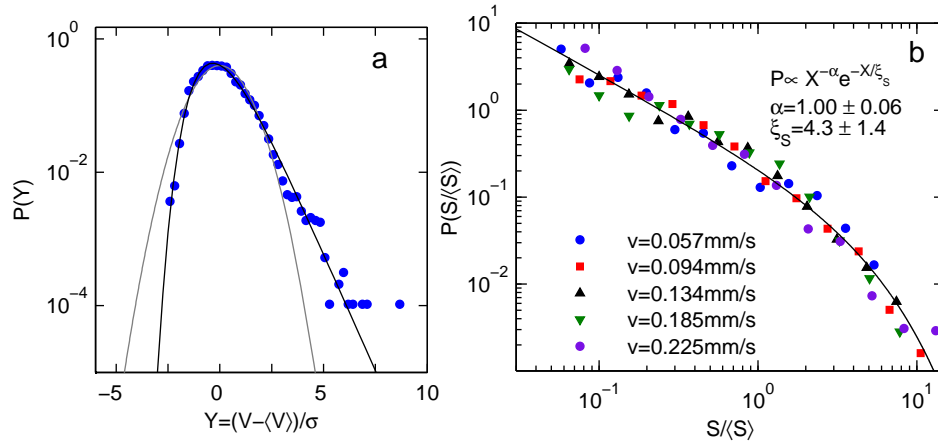


Figure 10. a) Distribution of the fluctuations of the front velocity for a low injection rate equal to $v = 0.057 \text{ mm/s}$ in an imbibition experiment. (b) Distributions of avalanches of the front velocity, normalized to the temporal average of the front velocity, for different injection rates (Courtesy of R. Planet and S. Santucci).

in the system. However, the explanation of the Gaussian distribution in the avalanches and its relation to the properties of the flow are questions that surpass the scope of this chapter.

Recently an experiment has been reported where both avalanches and fluctuations have been measured in an imbibition front [58]. A viscous liquid is injected into a Helle-Shaw cell where a random distribution of well controlled patches guarantees a specific level of disorder. The competition between viscous and capillary forces creates a jerky dynamics where the global velocity of the front displays avalanches that follow a scale invariant distribution fitted to an exponent -1 (figure 10b). The average of the avalanche size increases with the decrease of the injection rate ($v \rightarrow 0$) and as a consequence, the cutoff of the power-law moves to higher values of avalanche size, approaching a pure power-law in the limit ($v = 0$). The distribution of fluctuations also change from a Gaussian to a Gumbel as $v \rightarrow 0$ (figure 10a), indicating the critical properties of the system around $v = 0$. The authors have been able to relate the asymmetry of the Gumbel to the reduction of the degrees of freedom in the system as the velocity of the dynamics is reduced.

The main message of this part consists in revealing that power-law distributed avalanches are not a necessary condition in order to classify a system as *critical*, but different kinds of distributions can rule the avalanche behavior of an equilibrium system at the critical point. The question about the dynamics chosen by nature has been answered in the way that different dynamics have been observed in diverse phenomena; nevertheless, a general formalism capable of predicting the kind of dynamics for a particular phenomenon is still lacking. Concerning the question about CSD, although in both the Barkhausen and the imbibition experiments the critical point of the pinning-depinning transition is reached at a limit ($v \rightarrow 0$), the fact that the velocity of the dynamics is externally imposed leaves some doubts about the existence of CSD in real critical systems evolving through scale invariant avalanches. A stronger argument in favor of its existence comes from percolation, which shares many different points with a second order phase transition (including CSD) at the

percolation threshold, and where the avalanches are power-law distributed [66]. Another thing to retain from this part is the value of the exponent of the power-law displayed by a well established critical system in two dimensions.

4. Criticality in Scale Invariant Avalanches

4.1. Models without spatial structure

After the introduction in 1987 of the SOC [22] as a new critical phenomenon occurring in a class of dissipative coupled systems triggered by temporal fluctuations, many different approaches have been used in order to describe its dynamics. The first one corresponded to the *critical branching process* [25].

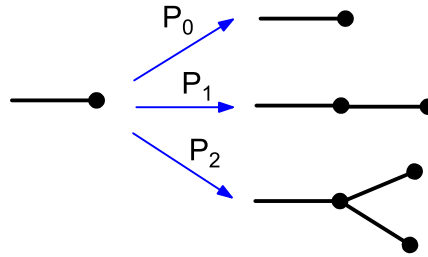


Figure 11. Branching process with $n_{max} = 2$.

The schema in figure 11 represents a branching process where each branch has a probability P_n of having n subbranches, $n \in [0, n_{max}]$. The different probabilities can be calculated by the following equations:

$$\sum_0^{n_{max}} nP_n = 1 + G \quad (24)$$

$$\sum_0^{n_{max}} P_n = 1 \quad (25)$$

where G corresponds to the average growth. *Criticality* is reached in the situation where the process barely “survives” [25], which corresponds to $G = 0$; i.e., it is the minimum probability able to develop branches proportional to the system size L ; where L is to the length where the process is artificially stopped. For $n_{max} = 2$, $P_0 = P_2 = (1 - P_1)/2$. If avalanches are defined as the number of generated branches, and the process is repeated a large number of times, the avalanche size distribution corresponds to a power-law with an exponent equal $-3/2$ and an exponential cut-off in the form

$$P(s) \sim s^{-3/2} \exp(-s/\lambda) \quad (26)$$

where $\lambda \sim L$ [67]. This result is in perfect agreement with the *mean-field theory* [27], with *percolation* in a Bethe lattice [66]; and also with recent works using *functional renormalization group* [70]. In the first two approaches there is no spatial structure. However, the same result appears if the processes take place in a real lattice, but only above a critical

dimension d_c . The higher the dimension, the less the probability for a branch to form a loop; and this absence of loops is a necessary conditions that makes the calculation possible. Unfortunately, $d_c = 4$ for the branching process [68, 69], and for the functional renormalization group [70]. For percolation $d_c = 6$ [66]. However, in real situations of two and three dimensions the results are different, and we will find values smaller than $-3/2$ for the critical exponents.

4.1.1. The role of dissipation and the structure of the avalanches

Although the solution displayed by eq. 26 works for spatial dimensions beyond the real world, it is very useful both for setting the lower limit to the critical exponents to $-3/2$, and for understanding the main concepts through discussion on an analytic base. By setting a negative value to G in eq. 24 it is possible to simulate the effect of the dissipation during the branching process: At every branching occasion, the probability is lower than the critical one; and as a result the average length of the branches decreases. The solution of the avalanche size distribution has the same shape (eq. 26), but with the difference that λ decreases with the dissipation, results that have also been reported in a Bethe lattice [71]. Dissipation reduces the size of the avalanches, and as a consequence the linear size of the mean avalanche is not proportional to the linear size of the system. λ is normally considered as the correlation length ξ , with the implication that the system is critical only in the conservative case.

There is a general belief that a dynamic of power-law distributed avalanches is a signature of a critical scenario (independently of the value of the exponent), and that the existence of a cut-off is the indication of the loose of critical properties. This consideration is based on the fact that, regardless the value of the exponent, eventually an avalanche is reaching the system size ($s_t \sim L$). However, in the analysis of the correlation length in section 3., the necessity of the temporal average has been presented. A particular avalanche (s_t) corresponds to a “microstate” in the dynamics, and a temporal average is needed in order to get the values of the physical magnitudes. Let us analyze this in detail:

The correlation length ξ has been defined in the eqs. 18 and 19; and the *criticality* of a system has been introduced as the divergence of the correlation length ($\xi \sim L$). The analysis of the Wolff algorithm in section 3.1.1. has shown a strong relation between structure and avalanche dynamics, suggesting that in a dynamics of scale invariant avalanches, it is possible to measure the *criticality* of the system through the average value of the avalanche sizes:

$$\langle s \rangle^{1/d_A} \sim L, \quad (27)$$

where d_A corresponds to the fractal dimension of the avalanche in a system of dimension d_S , and volume $V \sim L^{d_S}$. From eq. 10 one gets $\langle s \rangle \sim S_{max}^{b+2}$; therefore,

$$S_{max}^{(b_c+2)/d_A} \sim L \sim V^{1/d_S} \geq S_{max}^{1/d_S}, \quad (28)$$

$$(b_c + 2)d_S \geq d_A. \quad (29)$$

A larger value of the exponent b provokes a larger value of $\langle s \rangle$, and consequently it delivers larger avalanche sizes. By following the same principle of the branching process,

where the criticality was defined as the lower probability able to form branches reaching the system size, it seems possible to choose the smaller b_c . Consequently,

$$(b_c + 2)d_S = d_A. \quad (30)$$

The relation 30 links the critical exponent b_c to the difference between the fractal dimension of the avalanche and the dimension of the system. If $d_A = d_S$, the critical exponent is equal to -1 . In two and three dimensions, where the critical exponents in percolation [66] correspond to $-187/91 + 1 = -1.05$ and -1.18 , respectively; the relation 30 gives the values of $d_A = 1.9$ ($d_S = 2$) and $d_A = 2.46$ ($d_S = 3$), while the values presented by [66] correspond to $d_A = 91/48 = 1.89$ ($d_S = 2$) and $d_A = 2.53$ ($d_S = 3$). Although for two and three dimensions it seems to work, for the critical dimension $d_S = 6$, the relation gives a ratio $d_S/d_A = 2$, while the reported one is $3/2$ [66].

4.2. Avalanches in two and three dimensions

Above the critical dimension, different approaches have shown that the critical exponent of scale invariant avalanches corresponds to $-3/2$. Dissipation moves the cut-offs towards small avalanche size values, provoking a decrease in the mean value of avalanche sizes $\langle s \rangle$, thus breaking the criticality of the system. In two and three dimensions the situation is more complex: there is no universality in the values of the critical exponents, and dissipation can have different effects on the distribution, either changing the cut-off of the distribution [58] or decreasing the exponent of the power-law [1].

Figure 12 displays the critical exponents of the power-law distribution of avalanches for several models and in different dimensions. The models can be divided into three groups: percolation, Ising model, and slowly driven phenomena including the Olami-Feder-Christensen (OFC) [1] model, the BTW model [22] and the Manna model [72]. Percolation donates the highest exponent values, that decrease with the dimension until the critical dimension 6 where it reaches the value $-3/2$. The exponent value obtained in section 3.1.1.

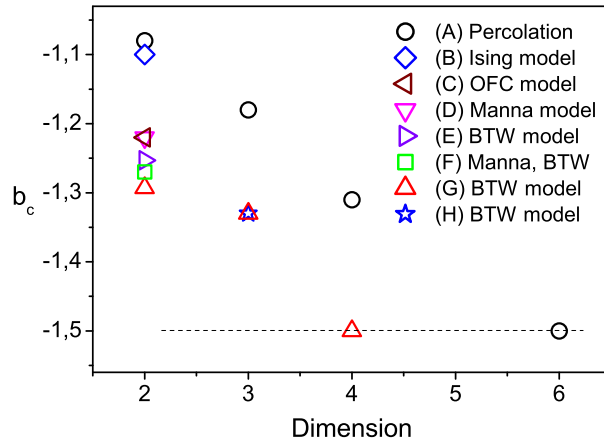


Figure 12. Critical exponents for several models with scale invariant avalanches in different dimensions: (A) [66], (B) Wolff algorithm (section 3.1.1.), (C) OFC model (conservative) [1], (D) [26], (E) [72], (F) [73], (G) [74], (H) [75].

by the avalanche distribution in the Ising model (Wolff algorithm) is also displayed and it shows a value close to Percolation in two dimensions. The group of slowly driven phenomena in two dimensions shows values approximately in the interval $(-1.3, -1.2)$, where there is also a report indicating universality with an exponent -1.27 between two of the presented models [73]. For three dimensions there are much less studies, but some numerical results indicate a critical exponent equal to -1.33 for the BTW model. As mentioned earlier, the critical dimension for slowly driven phenomena is 4 [27]. Following the relation 30, the different exponents must be related to the structure of the avalanches, in particular their fractal dimensions.

The lowest value of the critical exponent for the avalanches in slowly driven systems corresponds to $-3/2$ and takes place in dimension 4 (or superior). In three dimensions the results indicate a value equal to -1.33 and in two dimensions let us take -1.27 as the paradigm. However, the majority of real phenomena evolving through scale invariant avalanches present much lower exponents: earthquakes ($b = -2$), granular avalanches ($b = -1.6$) [12], superconducting vortices ($b = -1.6$) [15, 16, 17, 18], solar flares ($b = -1.8$) [14], subcritical fracture ($b = -1.5$) [19], and so on. Why do these phenomena “move” apart from the critical values of their respective dimensions? Dissipation is one possible answer.

The Olami-Feder-Christensen (OFC) model of earthquakes is a nonconservative model that mimics the behavior of two tectonic plates, and is able to tune the exponent of the power-law distribution of avalanches by modifying the degree of dissipation in the system [1]. Recent and still unpublished results in granular piles (the continuation of [12]) have shown the same tendency displayed by the OFC model: a decrease in the value of the exponent of the power-law distribution of avalanche sizes as dissipation increases. However, a quantitative relation between the dissipation and the exponent of the power-law is still lacking. Some reports have analyzed the effect of dissipation on the critical properties in the OFC model [76, 77, 78] and also in a more general framework [79]. The results show critical properties only in the conservative case; but again, a formalism linking the exponent

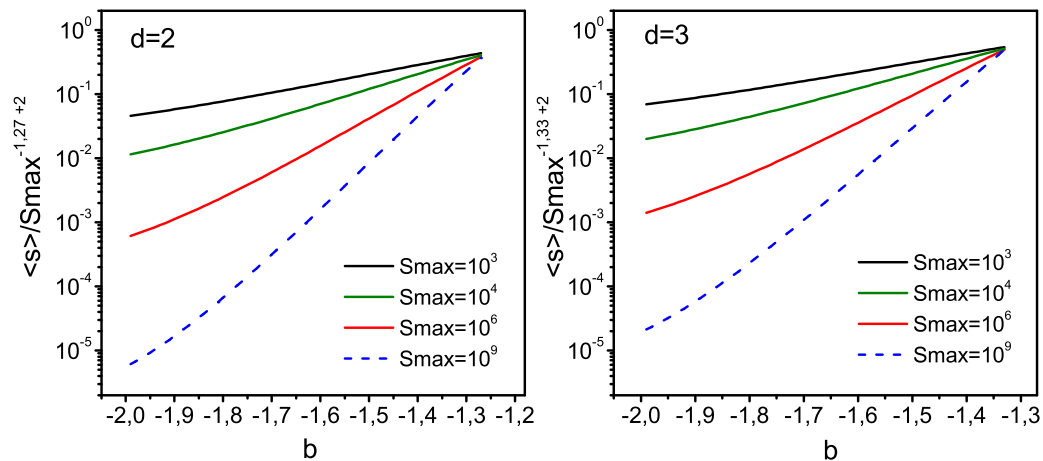


Figure 13. Results for the condition of criticality $\langle s \rangle / S_{max}^{b_c+2}$ for slowly driven systems in two and three dimensions.

of the power-law to the critical properties of the system is still missing. From the eqs. 27 and 28 it is possible to get a condition of criticality for scale invariant avalanches:

$$\frac{\langle s \rangle}{S_{max}^{b_c+2}} \sim 1 \quad (31)$$

with the considerations of $b_c = -1.27$ and $b_c = -1.33$ for two and three dimensions respectively, in the case of slowly driven systems. The results of this condition of criticality are displayed in figure 13, where the system separates exponentially from the critical situation as the exponent b decreases. For a given exponent the decrease grows linearly with the maximum avalanche size S_{max} .

In section 2.3.3. an energy balance limited the SOC in forbidding large values of b (close to -1) for dissipative slowly driven system. Now the results indicate that as the exponent decreases, which in different systems is a consequence of the dissipations, the system loses its critical properties. The combination of both results restrict SOC to conservative and critical models, like the original BTW one. This argument is in agreement with recent results in avalanche prediction, which is the main subject of the next section.

5. Towards Prediction and Control

Several works have claimed the unpredictable character of phenomena evolving through scale invariant avalanches (earthquakes, granular piles, solar flares, stock markets, etc) as a consequence of their classification as critical systems [44, 80]. However, in the last section it has been suggested that those systems are not critical, which is expressed in the small value of the exponent of their power-laws compared to the critical exponent at their respective dimensions. If they are not critical, they are, in principle, predictable; a fact that has been recently proved in both experiments and simulations.

5.1. Predicting scale invariant avalanches

The experiment studies the dynamics of avalanches in a quasi-two-dimensional granular pile [12]. It consists of a base of 60 *cm* row of randomly spaced 4 *mm* steel spheres, sandwiched between two parallel vertical glass plates 4.5 *mm* apart. The same steel beads are delivered one by one from a height of 28 *cm* above the base and at its center, resulting in the formation of a quasi-two-dimensional pile. The extremes of the base are open, leaving the beads free to abandon the pile. After a bead is delivered, the pile is recorded with a digital camera at a resolution of 21 pixels/bead-diameter, followed by the dropping of a new bead. One experiment contains more than 55000 dropping events with a total duration of more than 310 hours. The first 4500 events before the pile reaches a stationary state are not included in the statistics. The average number of beads in the pile is 3315. The centers of all the particles for each image are found, and the size of an avalanche is defined as the number of beads that has moved between two consecutive dropping events. The distribution of avalanches follows a power-law with an exponent $b = -1.6$ (figure 14a). Avalanches are classified as small, medium, large and extra-large; and the study focuses on predicting large and extra-large events. Foreshocks and aftershocks take place around large avalanches (figure 14b). However, these signs are rather weak, and all the efforts to predict *when* a large

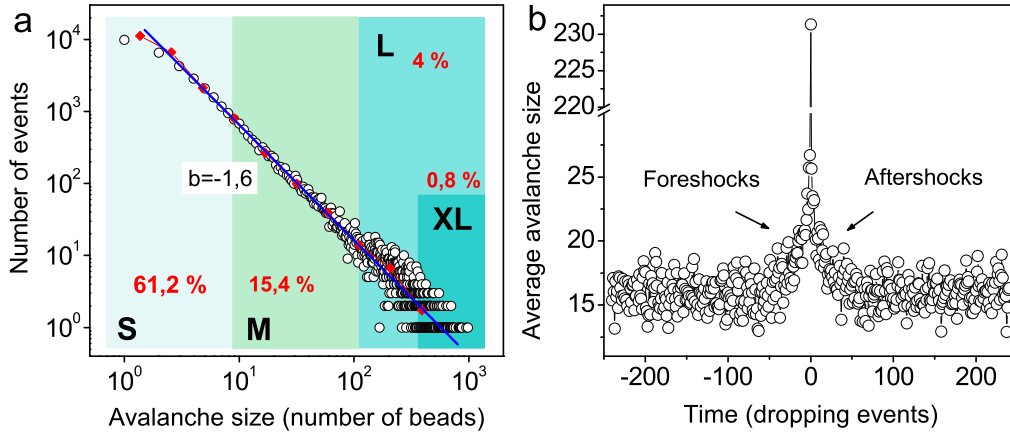


Figure 14. (a) Distribution of avalanche size for the granular experiment (circles). These points have been averaged with a logarithmic binning (diamonds) and they follow a power-law with an exponent $b = -1.6$. Avalanches have been classified as small (S), medium (M), large (L) and extra-large (XL). The percentage of occurrence of each type of avalanche is also displayed. (b) The average of the avalanche size around a large event (L) presents weak signs of foreshocks and aftershocks.

avalanche is going to happen did not succeed: the analysis of the time series does not allow the prediction of large events.

As the position of the centers of each particle at every step of the experiment is known, different structural variables can be defined and their evolution followed during all the experiment, particularly in the neighborhood of a large avalanche. The shape factor $\zeta = C^2/4\pi S$, where C is the perimeter and S the area of each voronoi cell in which the structure has been divided (figure 15a), has been computed at each step of the experiment. ζ is equivalent to the local disorder and inversely proportional to the packing fraction of the pile. The temporal cross-correlation between the shape factor (spatially averaged) and the large avalanches read as:

$$C(t) = \frac{\sum s_b(t_i)\zeta(t_i + t) - \langle s_b(t_i) \rangle \langle \zeta(t_i) \rangle}{\sqrt{\sum (s_b(t_i) - \langle s_b(t_i) \rangle)^2 \sum (\zeta(t_i) - \langle \zeta(t_i) \rangle)^2}} \quad (32)$$

where s_b corresponds to the binary series of large (extra-large) avalanches, i.e., 1 if the avalanche is large (extra-large) and 0 otherwise. The results are shown in figure 15b. The continuous variation displayed by the average disorder of the pile before a large event is very clear and approximately fifty steps before a large event, the average disorder continuously increases until the avalanche takes place. Then the pile reorganizes itself, but it gets trapped in an intermediate level of disorder. In the aftershocks zone, the disorder increases, and after that, the pile slowly evolves into more organized states. By using the information relative to the average disorder and the help of an extremely simple algorithm, it has been possible to reach up to 62% and 64% of success in the predictability of large and extra-large avalanches respectively. By changing the algorithm and adding more information these odds can be improved.

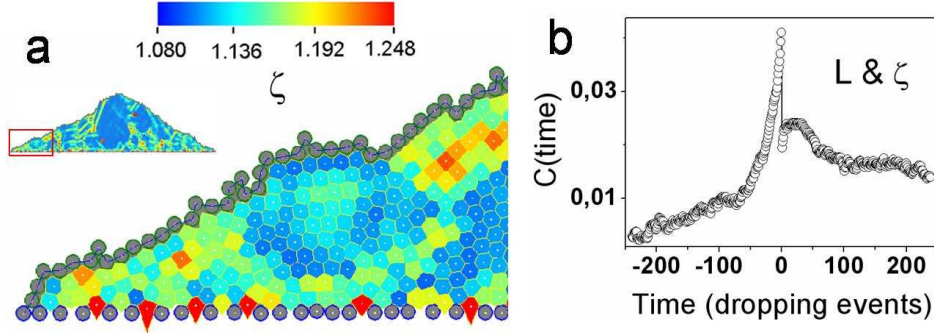


Figure 15. (a) Portion of the granular pile where the color of each voronoi cell represents the value of the shape factor. (b) Temporal cross-correlation between the large avalanches and the average shape factor.

Very similar results have been obtained in a more realistic modification of the OFC model [46, 81], consisting of a cellular automaton where the Burridge and Knopoff spring-block model has been mapped [82]. The spring-block model consists of a two dimensional array of blocks on a flat surface. Each block is connected by means of springs with its four nearest neighbours, and in the vertical direction, to a driving plate which moves horizontally at velocity v . When the force acting on a block overcomes the static friction of the surface, the block slips. A redistribution of forces then takes place in the neighbors that eventually triggers new displacements. In our model [81], the force on each block is stored in a site of the lattice, and the static friction thresholds are distributed randomly following a Gaussian. If 20% of the energy is lost in every redistribution of forces after one block slips, the distribution of avalanches resembles the Gutenberg-Richter law [83], showing a power-law with an exponent $b = -1.91$. The cross-correlation between the standard deviation of the force and the binary series of large avalanches donates a result very similar to the one presented in figure 15b for the granular experiment. The results are more pronounced for larger system sizes, indicating the possibility of prediction.

5.1.1. Criticality. Good or bad for prediction?

In a similar manner as in the Ising model, by following the eqs. 18 and 19, the correlation length ξ has been calculated and is presented in figure 16 [46]. As it is expected considering the low value of the exponent of the power-law $b = -1.91$, the average over regular intervals has donated a low value of the correlation length $\xi = 14$ in a system size $L = 128$; thus the system is not critical. The correlation length has also been calculated averaging the correlation functions at certain steps before (and after) a large event. The value of ξ calculated 300 steps before a large event corresponds to 36. This higher value seems to be an indication that in a temporal neighborhood preceding a large event, the system presents characteristics of a critical state, which has been denominated “*temporal critical state*” [46]. Therefore, if the average is performed over a “moving” and relatively small time window, the correlation length will have small values most of the time, but will eventually

reach values close to the system size in the neighborhoods of catastrophic events (temporal critical states). The existence of CSD in this temporary state could be extremely helpful in order to predict scale invariant avalanches [84]. Of course, inside the critical region it will not be possible to predict when a large avalanche will take place, but as the system size increases, the duration of this critical state must reduce. Concerning earthquakes, a report in 2009 has shown some measurements indicating a window duration of a few hours [85].

Our experiments and simulations present two major limitations: first, they are quasi-static, which makes impossible to analyze the existence of CSD. Second, the predictions are based on the internal structure, and although there are some studies claiming the possibility of predicting earthquakes following a similar idea [86, 87], the results are rather limited. However, there is an indirect sign indicating the existence of CSD in our experiment: the increase of disorder related to a reduction of the packing fraction in the system. In the percolation problem of the forest fires, the average termination time of the fire diverges at the percolation threshold [66]. At this critical point, the structure is connected in a complex way and we can imagine the spatial scenario as a labyrinth that the fire has to cross. In our system the increase of disorder related to a reduction of the packing fraction creates also a complex path, that can eventually slow down the “transfer of information” between different part of the system. In a more quantitative manner, in the jamming transition of a granular system, a decrease in the packing fraction provokes an increase of the soft modes [88] which are modes of very low frequency. This shift to low values in the frequency is equivalent to an increase of the correlation time (which is the signature of a CSD).

In the latest years, the possibility of continued measurements, storage and data analysis of several networks of seismometers and accelerometers has brought promising studies based mainly on the analysis of the cross-correlation function of the seismic noise [89, 90]. However, no precursors of large events have been found with this method; and probably the answer can also be found in the jamming transition, because the soft modes do not have any

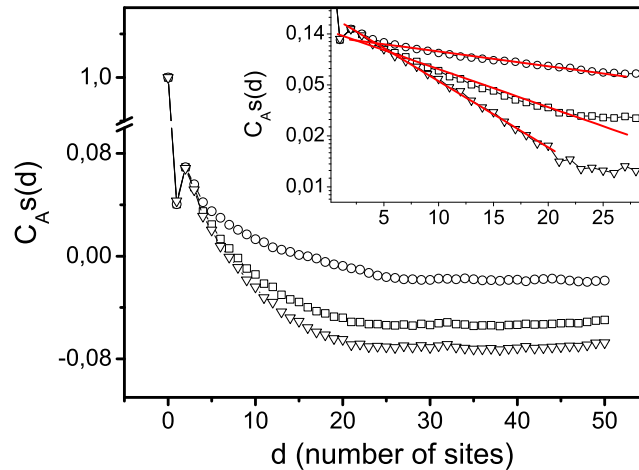


Figure 16. Averages of the spatial correlation function calculated at 300 steps before a large event (superior curve), 300 steps after a large event (inferior curve) and at equispaced intervals of 200 steps (middle curve), for $L=128$. (Inset) From a linear fit in log-lin axes, correlation length values equal to 36, 14 and 7 sites can be extracted.

influence on the elastic properties of the medium.

5.2. The origin of Scale invariant avalanches

The origin of the temporal scale invariance in nature has been a question of debate for more than two decades [24, 91, 92]. Being able to group many different phenomena (earthquakes, granular avalanches, solar flares, stock markets, etc) into the same kind of dynamics, where catastrophic events and small events are explained by the same principles, was an extraordinary achievement of the SOC. However, the axiomatic manner in which the base of the theory was introduced, related to the existence of a critical state as an attractor of the dynamics, set SOC as a theory to be proved more than as a theory to develop. This has provoked that several relevant questions concerning scale invariant avalanches have never been formulated in a direct manner; the influence of the dissipation and the influence of the disorder in the “self-organization” are examples of these questions.

Although there is not quantitative results about the two proposed questions, two decades of work on the subject have left some hints about them: the effect of the dissipation on modifying the exponent of the power-law has already been discussed in section 4.2.; and now let us analyze the influence of the disorder in the “self-organization” towards scale invariant avalanches. Two cases are going to be discussed: a granular pile and an earthquake model. In these situations (as well as all the other SOC systems) an energy gap controls the limits of the dynamics, i.e., the largest amount of dissipated energy. In the granular pile two angles define the energy gap: the subcritical angle and the supercritical angle [93]. In ideal conditions (little disorder and large friction) a trivial periodic behavior rules the dynamics [4, 94, 95, 96], charging and discharging the energy gap. In the earthquake model [1, 81] there is some elastic energy stored in every site of a lattice, which is limited by local thresholds related to a static friction coefficient. The largest possible avalanche happens when all the sites have reached their thresholds and, with the trivial condition of a flat distribution of thresholds, a trivial periodic behavior also rules the dynamics.

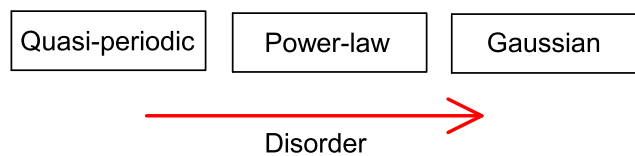


Figure 17. The disorder is able to modify the type of distribution in a system with an energy gap.

If the structural disorder in the granular pile is relevant, the periodicity is broken and avalanches become temporally uncorrelated with sizes distributed following a power-law [5, 6, 7]. In the case of the earthquake model, a more realistic Gaussian distribution of static friction thresholds will be sufficient in order to obtain a power-law distribution of events [81]; however, some signs of periodicity (proportional to the dissipation) are still present in the dynamics. By introducing more disorder (a Gaussian distribution of the values of the dissipation), the periodicity is broken while the avalanche size distribution remains as

a power-law. Nevertheless, increasing the values of the standard deviation of the Gaussian distribution will lead to the removal of the power-law behavior [81]. These simulations were focused on the SOC behavior; thus no more disorder was introduced after the rupture of the scale invariance; though it is evident that if a disorder is artificially increased, a Gaussian distribution behavior must be obtained. A simple example will be not respecting the separation of scales (drive and dissipation) required for a scale invariant behavior, and to drive continually a granular pile. The result will be a continuous flow and a Gaussian behavior will be obtained.

Predicting scale invariant avalanches in natural phenomena (particularly earthquakes), is one of the biggest challenges of today's science. However, predicting catastrophic avalanches it is not the final solution to this problem. The question to address is more practical: Is it possible to control scale invariant avalanches? The simplest solution in order to break the scale invariance is the *early triggering*, which is currently used in snow avalanches and in numerical models [97] to avoid large accumulations leading to catastrophic events. Understanding the role of dissipation, disorder, and other factors linked to the organization of a system into a dynamics of scale invariant avalanches, can be essential in the future development of tools leading to the control of catastrophic avalanches.

6. Conclusion

The essential role of the exponent value of the power-law distribution of avalanche sizes has been discussed. The exponent value controls the proportion between small and large events in the dynamics. For an exponent $b = -1$, for example, the probability of large and small events is the same (considering a logarithmic resolution). As the exponent value decreases (increases in absolute value), smaller events have more weight in the dynamics. This is also presented in the value of $\langle s \rangle$, related to the energy balance in the system, and forbidding exponents close to $b = -1$ for slowly driven systems. The exponent value also controls the critical properties of the system through the *condition of criticality* $\langle s \rangle / S_{max}^{b_c+2}$ where b_c corresponds to the critical exponent for slowly driven systems, with $b_c \sim -1.27$ and $b_c \sim -1.33$ in two and three dimensions respectively.

The causes, consequences, as well as some history of the logarithmic scale have also been presented. The logarithmic scale is the only scale that respects the scale invariance during the measurement. The fact that an integration is performed during the measurement changes the value of the exponent in +1 unit, which has provoked some confusion in the interpretation of the distribution of earthquakes. However, it has been shown that a power-law with an exponent $b = -2$, and the consideration of one earthquake occurring every 0.21 seconds, fits quite well the real data.

Simulation on a well established critical system (the Ising model) has revealed that power-law distributed avalanches are not a necessary condition in order to classify a system as *critical*, but different kinds of distributions can rule the avalanche behavior of an equilibrium system at the critical point: A "Metropolis" algorithm displayed avalanches distributed following a Gaussian, while the "Wolff" algorithm presented a scale invariant dynamics with a critical exponent $b = -1.1$. Different experiments have shown different kind of dynamics.

Real scale invariant phenomena (earthquakes, granular piles, solar flares, etc) normally present exponent values far from the critical ones, and simulations and table experiments suggest that dissipation is the cause of these low values. As the exponent moves apart from the the critical value, the *condition of criticality* indicates that the system is loosing the critical properties, thus it becomes, in principle, predictable. Prediction of scale invariant avalanches has been achieved both in a quasi-two-dimensional granular pile ($b = -1.6$) and in an earthquake model ($b = -1.91$). The correlation length ξ has been calculated in the earthquake model showing a low value when the correlation function is averaged over the whole dynamics (or non correlated events). However, if ξ is calculated averaging the correlation function over a small time window, it presents small values most of the time, but eventually it reaches values proportional to the system size preceding catastrophic events, a situation denominated “*temporal critical state*”. The analysis of this temporal state can eventually be used to forecast real catastrophic avalanches.

The influence of dissipation and disorder in the “self-organization” of scale invariant dynamics have been discussed in a qualitative manner. However, quantitative studies are still missing. These studies can eventually have an impact in the prediction and control of real catastrophic avalanches.

7. Acknowledgments

I am pleased to thank N. Arnesen and O. Duran for proofreading the manuscript; E. Altshuler, S. Ciliberto, O. Duran, P. Holdsworth, K. J. Måløy, T. Roscilde, S. Santucci and L. Vanel for useful discussions; J.-F. Pinton for sharing some experimental data; R. Planet and S. Santucci for providing the figure 10; and C. Creton and A. Lindner for a lot of support during the writing of this chapter. I am also pleased to thank Henrik Jeldtoft Jensen, who reviewed the manuscript and made very useful comments. This work has been financed by the European project MODIFY.

References

- [1] Olami, Z.; Feder, H. J. S.; Christensen, K. *Phys. Rev. Lett.* 1992, 68, 1244.
- [2] Bak, P.; Tang C. *J. Geophys. Res.* 1989, 94 (15) 635.
- [3] Jagla, E. A. *Phys. Rev. E* 2010, 81, 046117.
- [4] Held, A. et al. *Phys. Rev. Lett.* 1990, 65, 1120.
- [5] Frette, V. et al. *Nature* 1996, 379, 49.
- [6] Altshuler, E.; Ramos, O.; Martínez, C.; Flores, L. E.; Noda, C. *Phys. Rev. Lett.* 2001, 86, 5490.
- [7] Aegerter, C. M.; Günther, R.; Wijngaarden, R. J. *Phys. Rev. E* 2003, 67, 051306.
- [8] Costello, R. M. et al. *Phys. Rev. E* 2003, 67, 041304.

-
- [9] Nerone, N.; Aguirre, M. A.; Calvo, A.; Bideau, D.; Ippolito, I. *Phys. Rev. E* 2003, 67, 011302.
- [10] Aegerter, C. M.; Lőrincz, K. A.; Welling, M. S.; Wijngaarden, R. J. *Phys. Rev. Lett.* 2004, 92, 058702.
- [11] Lőrincz, K. A.; Wijngaarden, R. J. *Phys. Rev. E* 2007, 76, 040301(R).
- [12] Ramos, O.; Altshuler, E.; Måløy, K. J. *Phys. Rev. Lett.* 2009, 102, 078701.
- [13] Birkeland, K. W.; Landry, C. C. *Geophys. Res. Lett.* 2002, 29 (11), 1554.
- [14] Hamon, D.; Nicodemi, M.; Jensen, H. J. *Astron. Astrophys.* 2002, 387, 326334.
- [15] Bassler, K.; Paczuski, M. *Phys. Rev. Lett.* 1998, 81, 37613764.
- [16] Altshuler, E.; Johansen, T. H. *Rev. Mod. Phys.* 2004, 76, 471487.
- [17] Altshuler, E. et al. *Phys. Rev. B* 2004, 70, 140505(R).
- [18] Altshuler, E. et al. *Physica C* 2004, 501, 408-410.
- [19] Santucci, S.; Vanel, L.; Ciliberto, S. *Phys. Rev. Lett.* 2004, 93, 095505
- [20] Sneppen, K.; Bak, P.; Flyvbjerg, H.; Jensen, M. H. *PNAS* 1995, 92, 5209.
- [21] Lee, Y.; Nunes Amaral, L. A.; Canning, D.; Meyer, M.; Stanley, H. E. *Phys. Rev. Lett.* 1998, 81, 3275.
- [22] Bak, P.; Tang C.; Wiesenfeld K. *Phys. Rev. Lett.* 1987, 59, 381-384.
- [23] Jensen, H. J. *Self-Organized Criticality, Emergent Complex Behavior in Physical and Biological Systems*; Cambridge Univ. Press: Cambridge, 1998.
- [24] Bak, P. *How Nature works-The Science of Self-organized Criticality*; Oxford Univ. Press: Oxford, 1997.
- [25] Alstrøm, P. *Phys. Rev. A* 1988, 38, 4905-4906.
- [26] Pietronero, L.; Vespignani, A.; Zapperi, S. *Phys. Rev. Lett.* 1994, 72, 1690.
- [27] Vespignani, A.; Zapperi, S. *Phys. Rev. Lett.* 1997, 78, 4793-4796.
- [28] Mandelbrot, B. B. *Les Objets fractals, forme, hasard et dimension*; Flammarion: Paris, 1975.
- [29] Mandelbrot, B. B. *The Fractal Geometry of Nature*; W. H. Freeman & Co: San Francisco, CA, 1982.
- [30] Koch, H. V. In *Classics on Fractals*; Edgar, G. A.; Ed.; Addison-Wesley, Reading MA, 1993.
- [31] Gutenberg, B.; Richter, C. F. *Ann. Geophys.* 1956, 9, 1-15.

-
- [32] Peek, J. B. H.; Bergmans, J. W. M.; Haaren, J. A. M. M.; Toolenaar, F.; Stan, S. G. *Origins and Successors of the Compact Disc*; Eindhoven, 2009; Philips Research Book Series, Vol. 11.
- [33] Russ, J. C. *The image processing handbook*; CRS Press: Boca Raton, FL, 2002; pp 23.
- [34] Pogson, N. R. *Mon. Not. R. Astron. Soc.* 1856, 17, 12-15.
- [35] Ptolemy. First printed in *Almagestum Cl. Ptolemei*; Venice, 1515.
- [36] Toomer, G. T. In *Dictionary of Scientific Biography*; Gillespie, C. C.; Ed.; Charles Scribner, New York, 1978; Vol. 15, pp 207-224.
- [37] Fechner, G. T. *Elemente der Psychophysik*; Breitkopf und Härtel Leipzig, 1860.
- [38] Stevens, S. S. *Science* 1961, 133, 8086.
- [39] Richter, C. F. *Bull. Seismol. Soc. Am.* 1935, 25, 1-32.
- [40] Los Angeles Times. (October 01, 1985) Charles F. Richter Dies; Earthquake Scale Pioneer.
- [41] Richter, C. F. *Elementary Seismology*; W. H. Freeman & Co: San Francisco, CA, 1958; pp 135-149; 650-653.
- [42] Sethna, J. P. *Statistical Mechanics: Entropy, Order Parameters, and Complexity*; Clarendon press: Oxford, 2009; pp 265.
- [43] Bak, P.; Christensen, K.; Danon, L.; Scanlon, T. *Phys. Rev. Lett.* 2002, 88, 178501.
- [44] Main, I. *Nature Debate* 25 February to 8 April (1999). http://www.nature.com/nature/debates/earthquake/quake_frameset.html
- [45] U.S. Geological Survey (2010). Earthquake Facts and Statistics. <http://earthquake.usgs.gov/earthquakes/eqarchives/year/eqstats.php>
- [46] Ramos, O. *Tectonophysics* 2010, 485 321-326.
- [47] Pruesner, G.; Peters, O. *Phys. Rev. E* 2006, 73, 025106(R).
- [48] Stanley, H. E. *Introduction to Phase Transitions and Critical Phenomena*; Oxford Univ. Press: New York, 1987.
- [49] Clusel, M.; Fortin, J.-Y.; Holdsworth, P. C. W. *Phys. Rev. E* 2004, 70, 046112.
- [50] Newman, M. E. J.; Barkema, G. T. *Monte Carlo Methods in Statistical Physics*; Oxford Univ. Press: New York, 1999.
- [51] Onsager, L. *Phys. Rev.* 1944, 65, 117.
- [52] Stauffer, D. *Int. J. Mod. Phys. C* 1998, 9, 562.

-
- [53] Bramwell, S. T. et al. *Phys. Rev. Lett.* 2000, 84, 3744.
- [54] Bramwell, S. T.; Holdsworth, P. C. W.; Pinton, J.-F. *Nature* 1998, 396, 552.
- [55] Metropolis, N. et al. *J. Chem. Phys.* 1953, 21, 1087.
- [56] Wolff, U. *Phys. Rev. Lett.* 1989, 62, 361.
- [57] Joubaud, S.; Petrosyan, A.; Ciliberto, S.; Garnier, N. B. *Phys. Rev. Lett.* 2008, 100, 180601.
- [58] Planet, R.; Santucci, S.; Ortín, J. *Phys. Rev. Lett.* 2009, 102, 094502.
- [59] Dunlavy, M. J.; Venus, D. *Phys. Rev. B* 2005, 71, 144406.
- [60] Ciliberto, S. Private communication.
- [61] Sethna, J. P.; Dahmen, K. A.; Myers, C. R. In *Scale Invariance and Beyond*; Dubrulle, B.; Graner, F.; Sornette, D.; Ed.; Springer, Berlin, 1997, Les Houches Workshop, March 10-14, pp 87.
- [62] Sethna, J. P.; Dahmen, K. A.; Myers, C. R. *Nature* 2001, 410, 242.
- [63] Zapperi, S.; Cizeau, P.; Durin, G.; Stanley, H. E. *Phys. Rev. B* 1998, 58, 63536366.
- [64] Barkhausen, H. *Z Phys.* 1919, 20, 401.
- [65] Labbé, R.; Pinton, J.-F.; Fauve, S. *J. Phys. II France* 1996, 6, 1099-1110.
- [66] Stauffer, D; Aharony, A. *Introduction to Percolation Theory*; Taylor & Francis: London, 1994.
- [67] Harris, T. E. *The theory of branching processes*; Springer-Verlag: Berlin, 1963.
- [68] Obukhov, S. P. In *Random Fluctuations and Pattern Growth*; Stanley, H. E.; Ostrowsky, N.; Ed.; Kluwer, Dordrecht, 1988.
- [69] Díaz-Guilera, A. *Europhys. Lett.* 1994, 26, 177.
- [70] Le Doussal, P.; Wiese, K. J. *Phys. Rev. E* 2009, 79, 051106.
- [71] Lauritsen, K. B.; Zapperi, S.; Stanley, H. E. *Phys. Rev. E* 1996, 54, 2483-2488.
- [72] Manna, S. S. *J. Stat. Phys.* 1990, 59, 509.
- [73] Chessa, A.; Stanley, H. E.; Vespignani, A.; Zapperi, S. *Phys. Rev. E* 1999, 59, R12-R15.
- [74] Lübeck, S.; Usadel, K. D. *Phys. Rev. E* 1997, 56, 5138-5143.
- [75] Tang, C.; Bak, P. *Phys. Rev. Lett.* 1998, 60, 2347-2350.
- [76] Carvalho, J. X. de; Prado, C. P. C. *Phys. Rev. Lett.* 2000, 84, 4006.

- [77] Miller, G.; Boulter, C. J. *Phys. Rev. E* 2002, 66, 016123.
- [78] Xia, J.; Gould, H.; Klein, W.; Rundle, J. B. *Phys. Rev. E* 2008, 77, 031132.
- [79] Bonachela, J. A.; Muñoz, M. A. *J. Stat. Mech.* 2009, P09009, 1742-5468.
- [80] R. J. Geller, R. J.; Jackson, D. D.; Kagan, Y. Y.; Mulargia, F. *Science* 1997, 275, 1616.
- [81] Ramos, O.; Altshuler, E.; Måløy, K. J. *Phys. Rev. Lett.* 2006, 96, 098501.
- [82] Burridge, R.; Knopoff, L. *J. Geophys. Res. Bull. Seismol. Soc. Am.* 1967, 57, 341.
- [83] Christensen, K.; Olami, Z. *J. Geophys. Res.* 1992, 97, B6, 8729-8735.
- [84] Scheffer, M. et al. *Nature* 2009, 461, 53-59.
- [85] Manshour, P. et al. *Phys. Rev. Lett.* 2009, 102, 014101.
- [86] Crampin, S.; Gao, Y.; Peacock, S. *Geology* 2008, 36, 427-430.
- [87] Crampin, S.; Gao, Y. *Geophysical Journal International* 2010, 180, 1124.
- [88] Wyart, M.; Silbert, L. E.; Nagel, S. R.; Witten, T. A. *Phys. Rev. E* 2005, 72, 051306.
- [89] Brenguier, F. et al. *Science* 2008, 321, 1478.
- [90] Brenguier, F. et al. *Nature Geoscience* 2008, 1, 126.
- [91] Vespignani, A.; Zapperi, S. *Phys. Rev. E* 1998, 57, 6345.
- [92] Reed, W. J.; Hughes, B. D. *Phys. Rev. E* 2002, 66, 067103.
- [93] Daerr, A.; Douady, S. *Nature* 1999, 399, 241.
- [94] Jaeger, H. M.; Liu, C.; Nagel, S. R. *Phys. Rev. Lett.* 1989, 62, 4043.
- [95] Rosendahl, J.; Vekic, M.; Kelley J. *Phys. Rev. E* 1993, 47, 14011404.
- [96] Rosendahl, J.; Vekic, M.; Rutledge J. E. *Phys. Rev. Lett.* 1994, 73, 537540.
- [97] Cajueiro, D. O.; Andrade, R. F. S. *Phys. Rev. E* 2010, 81, 015102(R).